Optics Letters

Theory and measurement of the soliton self-frequency shift and efficiency in optical microcavities

Xu Yi,† Qi-Fan Yang,† Ki Youl Yang, and Kerry Vahala*

T. J. Watson Laboratory of Applied Physics, California Institute of Technology, Pasadena, California 91125, USA
**Corresponding author: vahala@caltech.edu*

Received 23 March 2016; revised 21 June 2016; accepted 27 June 2016; posted 27 June 2016 (Doc. ID 261694); published 19 July 2016

Dissipative Kerr cavity solitons experience a so-called self-frequency shift (SFS) as a result of Raman interactions. The frequency shift has been observed in several microcavity systems. The Raman process has also been shown numerically to influence the soliton pumping efficiency. Here, a perturbed Lagrangian approach is used to derive simple analytical expressions for the SFS and the soliton efficiency. The predicted dependences of these quantities on soliton pulse width are compared with measurements in a high-Q silica microcavity. The Raman time constant in silica is also inferred. Analytical expressions for the Raman SFS and soliton efficiency greatly simplify the prediction of soliton behavior over a wide range of microcavity platforms.

OCIS codes: (140.3945) Microcavities; (190.5650) Raman effect; (190.7110) Ultrafast nonlinear optics.

http://dx.doi.org/10.1364/OL.41.003419

Recently, a new type of temporal soliton, the dissipative Kerr cavity soliton, has been observed in both fiber [1] and microcavity resonators [2–6]. In microcavities, these solitons are being explored as possible routes to create a chip-based frequency comb system [7,8]. Like all optical solitons, dissipative Kerr cavity (DKC) solitons balance waveguide dispersion with the Kerr effect (intensity dependence of refractive index). Beyond this, however, DKC solitons also use the Kerr effect to compensate cavity loss through parametric amplification [2].

While the Kerr effect is essential to soliton formation, other nonlinearities can alter soliton properties. Soliton interaction with the Raman nonlinearity causes the so-called self-frequency shift (SFS). In optical fiber transmission, this effect causes the soliton's central frequency to experience increasing redshifting with propagation distance [9]. Intuitively, this is understood as a continuous energy transfer from the blue to red side of the soliton spectrum that is mediated by the Raman interaction [10]. The effect is of practical importance in supercontinuum generation using optical fibers [11]. It has also been used in difference frequency generation of mid-IR frequency combs [12]. Recently, the Raman SFS has been numerically modeled [13] and observed to influence DKC solitons [3,14]. Here, rather than producing a continuously increasing redshift, the Raman effect produces a constant frequency offset between the optical pump and the soliton spectral maximum (i.e., a frequency locked Raman soliton [13]). Without the Raman SFS, the optical pump would be centered on the soliton comb spectrum (at the spectral maximum). Instead, the soliton spectral maximum is red-shifted away from the pump. The amount of shift increases with soliton peak power and, so far, has been numerically calculated [3,13,14] by solving the Lugiato–Lefever equation [15].

Here, we present an analysis of the SFS for DKC solitons using the perturbed Lagrangian formalism and develop an analytical expression for the frequency shift in terms of soliton and cavity properties. In addition, an analytical expression for the soliton efficiency, including the Raman effect, is found and compared with new measurements, as well as those reported earlier [3]. The Raman SFS and soliton efficiency expressions are first compared with measurements to confirm the predicted behavior; then the derivation of these expressions is outlined.

To form DKC solitons, a microresonator must have a transverse mode family with dispersion that is both anomalous and free of avoided mode crossings [16]. Pumping of a single mode belonging to this mode family will generate solitons when the pumping frequency is red detuned relative to the mode resonance. Further details on the excitation of DKC solitons are provided in [2–6]. DKC solitons were generated in a 3 mm silica resonator (free spectral range ≈22 GHz). General information on the resonators and the techniques used to measure the solitons are described in [3,17]. Soliton spectra measured in a silica microresonator at two different operating points are shown in Fig. 1(a). Soliton generation is confirmed by time domain intensity autocorrelation and frequency resolved optical gating (FROG) [3]. Additional confirmation is provided by fitting to the theoretically predicted hyperbolic secant-squared spectrum [see the spectral envelopes in Fig. 1(a)]. The Raman SFS offset of the pump line relative to the soliton spectral center is also indicated in the figure. It can be seen that the broader soliton spectrum (narrower pulse width) features a larger Raman SFS. Finally, soliton pulse width, power, and Raman SFS depend on a single operating point parameter,

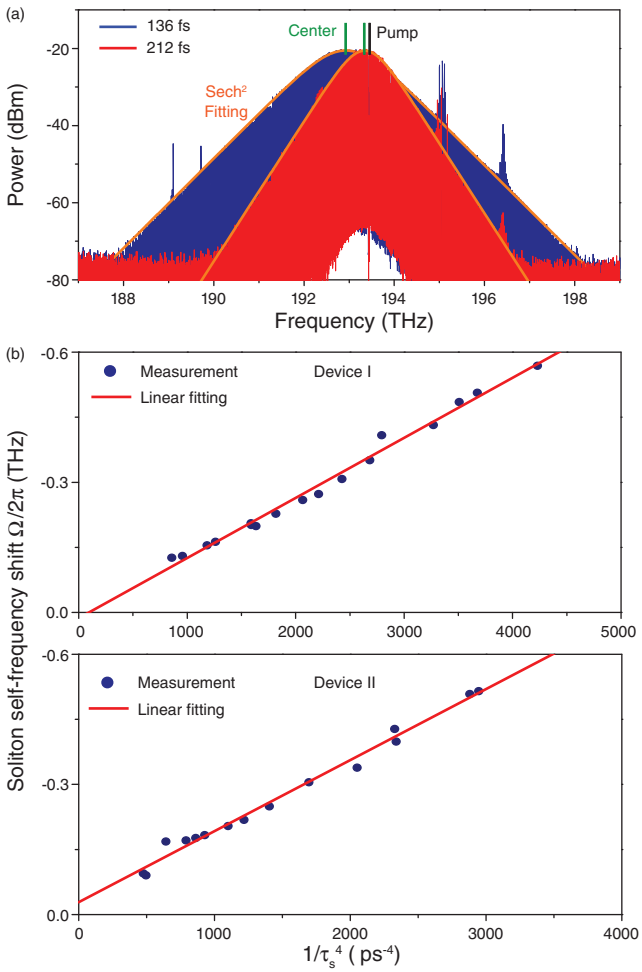

Fig. 1. (a) Optical spectra measured for a dissipative Kerr cavity soliton at two operating points. The pump power is suppressed using a fiber grating filter. A sech^2 fit is shown (orange curves), and pulse widths inferred from the fitting are shown in the legend. The location of the pump line is indicated as the black line. The centers of the spectra are indicated by the green lines. (b) Measured Raman SFS plotted versus $1/\tau_s^4$ for two devices. The red line is a linear fit according to Eq. (1).

the frequency detuning of the resonator mode being pumped relative to the pump frequency, $\delta\omega = \omega_0 - \omega_p$. ($\omega_p$ is the pump frequency, and ω_0 is the frequency of the resonator mode that is pumped.) To set and hold this parameter (and, in turn, other soliton properties), soliton power was used to servo control the pump laser frequency as described elsewhere [3,17]. In the measurements, the protocol was to hold frequency detuning close to the soliton existence maximum detuning [2,3] and to then vary this maximum detuning by adjusting the pumping power.

The key theoretical results of this Letter are the following expressions for the Raman SFS, Ω; the minimum input pump power required to generate a soliton, P_{min}; and the soliton pumping efficiency, $\Gamma = P_{\text{sol}}/P_{\text{min}}$ [18] (P_{sol} is the average soliton power):

$$\Omega = -\frac{8D_2 Q\tau_R}{15\omega_0 D_1^2}\frac{1}{\tau_s^4} = \frac{8c\tau_R Q\beta_2}{15n_0\omega_0}\frac{1}{\tau_s^4}, \quad (1)$$

$$P_{\text{min}} = P_0 \cosh^2\frac{\pi\Omega\tau_s}{2}, \quad (2)$$

$$\Gamma = \Gamma_0\,\text{sech}^2(\pi\Omega\tau_s/2), \quad (3)$$

where c, n_0, n_2 and β_2 are the speed of light, refractive index, Kerr nonlinear refractive index coefficient, and group velocity dispersion, respectively. $D_1/2\pi$ is the cavity-free spectral range in Hertz units at the pumping mode (i.e., soliton repetition frequency). Q (Q_E) is the total (external) optical Q factor and $\eta = Q/Q_E$ is the coupling factor. In addition, τ_s is the soliton pulse width, τ_R is the Raman time constant [19], and $D_2/2\pi$ gives the second-order dispersion in units of change in free-spectral range per mode ($D_2 = -\frac{c}{n_o}D_1^2\beta_2$). In addition, P_0 and Γ_0 are the soliton minimum pumping power and soliton efficiency in the absence of the Raman SFS (i.e., $\Omega = 0$) and are given by [3]:

$$P_0 = -\frac{2c}{\pi}\frac{A_{\text{eff}}\beta_2}{\eta n_2 Q D_1}\frac{1}{\tau_s^2}, \quad (4)$$

$$\Gamma_0 = \pi\eta^2 D_1\tau_s, \quad (5)$$

where A_{eff} is the effective nonlinear mode area. Before deriving Eqs. (1)–(3), they are compared with measurements.

To test the theory, a series of soliton spectra of increasing spectral width were obtained using the operating point locking method [17]. The Raman SFS, Ω, and the pulse width, τ_s, were measured by least-squares fitting of the soliton optical spectrum [see Fig. 1(a)] to the theoretical soliton spectral envelope $P(\omega) = P_c\,\text{sech}^2[\pi\tau_s(\omega - \omega_p - \Omega)/2]$, where P_c is the spectral maximum power. Figure 1(b) plots the measured Ω versus $1/\tau_s^4$ in two devices. For reference, device I is a device characterized previously [3]. A linear fitting to the two sets of data is also provided, confirming the predicted theoretical dependence in Eq. (1). Furthermore, with measured parameters (device I: $Q = 200$ million, $D_1/2\pi = 22$ GHz, $D_2/2\pi = 17$ kHz; and device II: $Q = 235$ million, $D_1/2\pi = 22$ GHz, $D_2/2\pi = 17$ kHz), a value of $\tau_R = 1.8$ fs, both for device I and for device II, is inferred from the linear fitting, which is in a reasonable agreement with the value of 2–4 fs reported in silica optical fibers [19]. The small non-zero intercept of the linear fitting is in the range of 1 free-spectral range (22 GHz) of the two resonators.

To measure the soliton efficiency, Γ, the operating point is fixed (i.e., laser-cavity detuning $\delta\omega$ is fixed) while the pump power is decreased until the soliton disappears. Near the disappearance point, the soliton average power, P_{sol}, and the minimum pump power, P_{min}, are recorded and used to obtain efficiency as $\Gamma = P_{\text{sol}}/P_{\text{min}}$. The pulse width is obtained from the optical spectrum as before. Measured efficiency is plotted versus the pulse width in Fig. 2 for devices I and II. The prediction given by Eq. (3) is shown as the solid line. The value of τ_R used in the plots is that inferred from fitting in Fig. 1(b). Also, $\eta = 0.29, 0.37$ for devices I and II. Device II has a higher efficiency as a result of a larger coupling coefficient. The agreement between the theory and measurement in Fig. 2(b) is very good, especially considering that there are no free parameters. The dashed lines in the plots give the uncorrected efficiency prediction of Eq. (5) (i.e., Γ_0 versus τ_s).

The derivation of Eqs. (1)–(3) is now presented. For transverse mode families that are relatively free of avoided mode crossings, the slowly varying internal cavity field $A(T, t)$ can

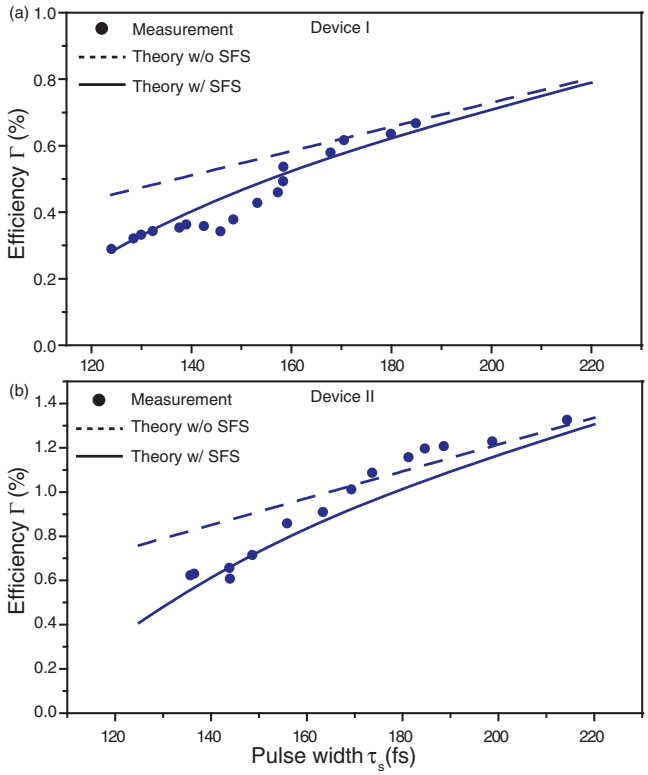

Fig. 2. Measured efficiency versus soliton pulse width is plotted (blue points) for two devices and compared with theory. A theory comparison with Raman (solid blue lines) and without Raman (dashed blue lines) is presented. There are no free parameters in the comparison. The small deviations between the measurement and the theory could result from the presence of weak avoided mode crossings in the dispersion spectrum [16].

be described by the Lugiato–Lefever equation [15] augmented with an additional Raman effect term [3,13,14]:

$$i\frac{\partial A}{\partial T}-\frac{c\beta_2}{2n_o}\frac{\partial^2 A}{\partial t^2}+g|A|^2A=-\left(i\frac{\kappa}{2}-\delta\omega\right)A+i\sqrt{\frac{\kappa\eta P_{\text{in}}}{\hbar\omega_o}}+g\tau_R A\frac{\partial|A|^2}{\partial t}, \tag{6}$$

where T and t are the slow and fast times, $g=\hbar\omega_o^2 n_2 D_1/2\pi n_o A_{\text{eff}}$ denotes the normalized Kerr effect nonlinear coefficient, $\kappa=\omega_0/Q$ is the power dissipation rate of the soliton mode family, and P_{in} is the pump power. Exact solutions of Eq. (6) are only known in the absence of dissipation and the Raman effect [20,21]. However, an approximate solution, including the dissipation term, has been calculated using the Lagrangian perturbation approach [22,23]. Here, we extend this method by including the Raman term as a perturbation.

The Lagrangian density for this system is given by [22–24]

$$\mathcal{L}=\frac{i}{2}\left(A^*\frac{\partial A}{\partial T}-A\frac{\partial A^*}{\partial T}\right)+\frac{c\beta_2}{2n_o}\left|\frac{\partial A}{\partial t}\right|^2+\frac{1}{2}g|A|^4-\delta\omega|A|^2, \tag{7}$$

and the dissipation, pumping, and Raman terms are combined in a perturbation $\mathcal{R}$, where

$$\mathcal{R}=-\frac{i\kappa}{2}A+i\sqrt{\frac{\kappa\eta P_{\text{in}}}{\hbar\omega_o}}+g\tau_R A\frac{\partial|A|^2}{\partial t}. \tag{8}$$

Equation (6) is recovered by taking $\delta\mathcal{L}/\delta A^*=\mathcal{R}$ [24]. The form for the slowly varying field envelope of the solitons wherein the central frequency is shifted by Ω is given by

$$A=B\,\text{sech}[(t-t_o)/\tau_s]e^{-i\Omega(t-t_o)}e^{i\phi}, \tag{9}$$

which is an exact solution for the case with no perturbation ($\mathcal{R}=0$). This form is also consistent with measurement and numerical modeling of the DKC solitons in the presence of Raman interactions [3,13,14]. For the proceeding analysis, the soliton phase (ϕ), temporal position (t_o), amplitude (B), pulse width (τ_s), and shift frequency (Ω) are considered functions of T, the slow time variable. Finally, Eq. (9) assumes $\delta\omega\gg\kappa$ (i.e., large pump detuning). In this case, the background field associated with DKC solitons is much weaker than the soliton peak power and is not included in Eq. (9). However, it can be retrieved from Eq. (6) for $|(t-t_0)/\tau_s|\gg 1$, where the soliton pulse is no longer dominant [2,23,25].

It is observed experimentally that the central soliton comb line power is a constant (independent of the operating point) and in good agreement with the Raman-free Lugiato–Lefever prediction [3]. By Fourier transform of a train of periodic pulses (period $=2\pi/D_1$) of the form in Eq. (9), the power per comb line at the central maximum of the soliton spectrum is given by $\hbar\omega_0^2 D_1^2/4Q_{\text{ext}}\times B^2\tau_s^2$. Accordingly, to be consistent with experimental observations, the product $B\tau_s$ is assumed to be given by the Raman-free result, $B\tau_s=\sqrt{-c\beta_2/gn_o}$. This is used to eliminate τ_s in the calculation below. It is also possible to show that this result follows directly from variation of the Raman-perturbed system [Eqs. (7) and (8)] with B and τ_s treated as independent variables.

The equations of motion for the perturbed Lagrangian have the form [23–25],

$$\frac{\partial L}{\partial r_i}-\frac{d}{dT}\frac{\partial L}{\partial \dot{r}_i}=\int\left(\mathcal{R}\frac{\partial A^*}{\partial r_i}+\mathcal{R}^*\frac{\partial A}{\partial r_i}\right)dt, \tag{10}$$

where the coordinates r_i in the Lagrangian are taken as the parameters B, Ω, t_o, and ϕ. Using Eq. (9) in the Lagrangian density, Eq. (7) gives the following result:

$$L=\int\mathcal{L}dt=2B\sqrt{\frac{-c\beta_2}{gn_o}}\left(\frac{gB^2}{6}+\frac{c\beta_2\Omega^2}{2n_o}-\delta\omega-\Omega\frac{\partial t_0}{\partial T}-\frac{\partial\phi}{\partial T}\right). \tag{11}$$

Inserting Eqs. (9) and (11) into Eq. (10) yields the equations of motion for parameters B, t_o, Ω, and ϕ:

$$\frac{dB}{dT}=-\kappa B+\pi\sqrt{\frac{\kappa\eta P_{\text{in}}}{\hbar\omega_o}}\cos\phi\,\text{sech}\left(\sqrt{\frac{-c\beta_2}{gn_0}}\frac{\pi\Omega}{2B}\right), \tag{12}$$

$$\frac{d\phi}{dT}=\frac{g}{2}B^2-\delta\omega+\frac{c\beta_2}{2n_0}\Omega^2-\frac{\partial t_o}{\partial T}\Omega, \tag{13}$$

$$\frac{dB\Omega}{dT}=-\kappa B\Omega+\frac{8n_0\tau_R g^2}{15c\beta_2}B^5, \tag{14}$$

$$\frac{dt_o}{dT}=\frac{c\beta_2}{n_0}\Omega, \tag{15}$$

where $\delta\omega\gg\kappa$ and (to be consistent with the measurement protocol) operation near the soliton maximum existence detuning are assumed. The latter is equivalent to assuming ϕ is near zero in the analysis. Equation (15) corresponds to the change of

soliton repetition rate due to the SFS [22] and has recently been observed [26]. The steady-state solution of Eq. (14) gives Eq. (1) for the SFS Ω (also using $B\tau_s = \sqrt{-c\beta_2/gn_o}$), while Eqs. (12) and (13) give the following steady-state results:

$$B = \sqrt{\frac{-c\beta_2}{gn_o}}\frac{1}{\tau_s} = \sqrt{\frac{2}{g}\left(\delta\omega + \frac{c\beta_2}{2n_o}\Omega^2\right)}, \tag{16}$$

$$\cos\phi = \frac{1}{\pi\tau_s}\sqrt{\frac{-c\beta_2\kappa\hbar\omega_o}{\eta g n_o P_{\text{in}}}}\cosh\frac{\pi\Omega\tau_s}{2}. \tag{17}$$

Combining Eqs. (1) and (16), the SFS and soliton pulse width can be related to the laser-cavity detuning,

$$\delta\omega = \sqrt{\frac{15c\beta_2\omega_0}{32n_oQ}}\frac{\Omega}{\tau_R} - \frac{c\beta_2}{2n_o}\Omega^2, \tag{18}$$

$$\delta\omega = -\frac{c\beta_2}{2n_o}\frac{1}{\tau_s^2}\left(1 + \frac{64c^2\tau_R^2Q^2\beta_2^2}{225n_o^2\omega_0^2}\frac{1}{\tau_s^6}\right). \tag{19}$$

It is important to remember that despite the form of these equations, detuning ($\delta\omega$) is the parameter that is controlled in a measurement. In addition, in Eq. (18), note that in the limit of $\tau_R \to 0$, $\Omega \to 0$ for finite $\delta\omega$.

The minimum input power for soliton existence given by Eq. (2) can be obtained by requiring $|\cos\phi| \le 1$ in Eq. (17). The average soliton power is given by [2,3]

$$P_{\text{sol}} = -\frac{2c\eta A_{\text{eff}}\beta_2}{n_2Q}\frac{1}{\tau_s}. \tag{20}$$

This expression follows from Eq. (9) and the relation between B and τ_s noted above. Using Eqs. (2) and (20), the soliton efficiency in Eq. (3) can be obtained from $\Gamma = P_{\text{sol}}/P_{\text{min}}$.

By numerical simulation of Eq. (6), the relations among Ω, τ_s, and $\delta\omega$ given by Eqs. (1), (18), and (19) were confirmed for both the silica resonator in this Letter and for silicon nitride resonators (parameters as in [14]: $D_1/2\pi =$ 100 GHz, $D_2/2\pi = 2$ MHz, $\kappa/2\pi = 350$ MHz, and $\tau_R =$ $0.2 \times 20/2\pi = 0.64$ fs). The form of the Raman interaction used here assumes that higher order terms beyond the shock term are negligible. This imposes a restriction on pulse times to be much longer than the damping time of vibrations [27]. This assumption is satisfied here. Finally, even though the behavior of the Raman SFS in microcavities differs in comparison to conventional soliton propagation in optical fiber (i.e., frequency locking behavior in microcavities [13]), it is interesting to note that both systems exhibit an inverse quartic dependence on soliton pulse width [10].

In summary, closed-form expressions for the Raman self-frequency-shift and the efficiency of dissipative Kerr cavity solitons have been derived using the Lagrangian perturbation approach. The results are in good agreement with measurements in silica microcavities. The expressions should be applicable to predict soliton behavior in any microcavity system.

Funding. Defense Advanced Research Projects Agency (DARPA) under the QuASAR and PULSE programs; National Aeronautics and Space Administration (NASA); Kavli Nanoscience Institute; National Science Foundation (NSF) Institute for Quantum Information and Matter, a NSF Physics Frontiers Center; Gordon and Betty Moore Foundation.

Acknowledgment. The authors thank Xueyue Zhang for checking the derivations in this paper and for confirming that the relation between B and τ_s follows from variation of the Raman-perturbed system.

[†]These authors contributed equally to this work.

REFERENCES

1. F. Leo, S. Coen, P. Kockaert, S.-P. Gorza, P. Emplit, and M. Haelterman, Nat. Photonics **4**, 471 (2010).
2. T. Herr, V. Brasch, J. Jost, C. Wang, N. Kondratiev, M. Gorodetsky, and T. Kippenberg, Nat. Photonics **8**, 145 (2014).
3. X. Yi, Q.-F. Yang, K. Y. Yang, M.-G. Suh, and K. Vahala, Optica **2**, 1078 (2015).
4. V. Brasch, M. Geiselmann, T. Herr, G. Lihachev, M. Pfeiffer, M. Gorodetsky, and T. Kippenberg, Science **351**, 357 (2016).
5. P.-H. Wang, J. A. Jaramillo-Villegas, Y. Xuan, X. Xue, C. Bao, D. E. Leaird, M. Qi, and A. M. Weiner, Opt. Express **24**, 10890 (2016).
6. C. Joshi, J. K. Jang, K. Luke, X. Ji, S. A. Miller, A. Klenner, Y. Okawachi, M. Lipson, and A. L. Gaeta, Opt. Lett. **41**, 2565 (2016).
7. P. Del'Haye, A. Schliesser, O. Arcizet, T. Wilken, R. Holzwarth, and T. Kippenberg, Nature **450**, 1214 (2007).
8. T. J. Kippenberg, R. Holzwarth, and S. Diddams, Science **332**, 555 (2011).
9. F. M. Mitschke and L. F. Mollenauer, Opt. Lett. **11**, 659 (1986).
10. J. P. Gordon, Opt. Lett. **11**, 662 (1986).
11. J. M. Dudley, G. Genty, and S. Coen, Rev. Mod. Phys. **78**, 1135 (2006).
12. A. Gambetta, R. Ramponi, and M. Marangoni, Opt. Lett. **33**, 2671 (2008).
13. C. Milián, A. V. Gorbach, M. Taki, A. V. Yulin, and D. V. Skryabin, Phys. Rev. A **92**, 033851 (2015).
14. M. Karpov, H. Guo, A. Kordts, V. Brasch, M. H. Pfeiffer, M. Zervas, M. Geiselmann, and T. J. Kippenberg, Phys. Rev. Lett. **116**, 103902 (2016).
15. L. A. Lugiato and R. Lefever, Phys. Rev. Lett. **58**, 2209 (1987).
16. T. Herr, V. Brasch, J. Jost, I. Mirgorodskiy, G. Lihachev, M. Gorodetsky, and T. Kippenberg, Phys. Rev. Lett. **113**, 123901 (2014).
17. X. Yi, Q.-F. Yang, K. Youl, and K. Vahala, Opt. Lett. **41**, 2037 (2016).
18. C. Bao, L. Zhang, A. Matsko, Y. Yan, Z. Zhao, G. Xie, A. M. Agarwal, L. C. Kimerling, J. Michel, L. Maleki, and A. E. Willner, Opt. Lett. **39**, 6126 (2014).
19. A. Atieh, P. Myslinski, J. Chrostowski, and P. Galko, J. Lightwave Technol. **17**, 216 (1999).
20. I. Barashenkov and Y. S. Smirnov, Phys. Rev. E **54**, 5707 (1996).
21. A. Matsko, A. Savchenkov, W. Liang, V. Ilchenko, D. Seidel, and L. Maleki, Opt. Lett. **36**, 2845 (2011).
22. A. B. Matsko and L. Maleki, Opt. Express **21**, 28862 (2013).
23. T. Herr, M. L. Gorodetsky, and T. J. Kippenberg, "Dissipative Kerr solitons in optical microresonators," arXiv:1508.04989 (2015).
24. A. Hasegawa, IEEE J. Sel. Top. Quantum Electron. **6**, 1161 (2000).
25. P. Grelu, *Nonlinear Optical Cavity Dynamics: from Microresonators to Fiber Lasers* (Wiley, 2015).
26. Q.-F. Yang, X. Yi, K. Y. Yang, and K. Vahala, "Spatial-mode-interaction-induced dispersive-waves and their active tuning in microresonators," arXiv:1606.00954 (2016).
27. G. P. Agrawal, *Nonlinear Fiber Optics* (Academic, 2007).